Light and Elevated Temperature Induced Degradation (LeTID) in a Utility-scale Photovoltaic System

Michael G. Deceglie, Timothy J Silverman, Steve W. Johnston, Jim Rand, Mason Reed, Robert Flottemesch, Ingrid L. Repins

***Abstract*—We present a detailed case study of degradation in a monocrystalline photovoltaic modules operating in a utility-scale power plant over the course of approximately three years. We present the results of degradation analysis on arrays within the sites, and find that five of the six arrays degraded faster than the best performing array. We also describe the results of extensive laboratory characterization of modules returned from the field, including module- and cell-level current-voltage characterization, luminescence imaging, and accelerated testing. The laboratory test results and field performance are consistent with LeTID. This paper also demonstrates a method to identify possible LeTID degradation in the field and confirm the result with laboratory testing of a small number of modules.**

***Index Terms*—Photovoltaics, LeTID, degradation, open-source, reliability**

I. Introduction

In order to have accurate models for photovoltaic (PV) system energy generation and financial performance it is critical to accurately predict degradation. When degradation occurs more rapidly than expected, equipment manufacturers need to know to address the problem for future products. Similarly, system owners need to know to bring their performance and financial models in line with reality, or how to utilize procurement practices that can achieve the desired reality. These instances also provide an opportunity to improve standards (e.g. [1]) to catch emerging degradation modes.

In recent years, a degradation mode termed light and elevated temperature induced degradation (LeTID) has emerged in Si solar cells, and has been shown to be distinct from previously known effects such as light-induced degradation (LID) [2], [3]. LeTID has been observed in a variety of Si-based PV technologies [2], [4]–[6].

We report a case study of degradation observed in a utility scale photovoltaic power plant operating in the Mid-Atlantic United States that exhibits features consistent with LeTID. The power plant was identified as an under-performing system by its owner through performance models using measured time series data in combination with plant availability. High availability yet low performance suggested a potential DC capacity issue. We present the results of a study of the time series energy generation data and a detailed laboratory analysis of sample modules returned from the site. Field characterization combined with time series degradation analysis identified which of modules were degrading faster than expected and which were performing normally. We used these results to identify a small set of modules of both under-performing and "good" modules for laboratory characterization to identify the degradation rate and mechanism. This approach enabled us to construct a detailed case study of the system and determine the root cause of reduced energy yield.

We begin with a description of the system and field observations, then proceed with an explanation of the methods employed in the time series analysis and laboratory characterization. The laboratory characterization methods used here include electroluminescence (EL), photoluminescence (PL), module- and cell-level current voltage (IV) characterization under simulated sunlight. We then describe the results in two subsections, the first focuses on the evolution of energy generation in the field and the state of modules as they were received from the field. The second describes the effects of an accelerated test known to accelerate LeTID and the subsequent associated recovery. Finally we describe how our results are consistent with LeTID.

II. System description and field observations

This study concerns a utility-scale solar photovoltaic power plant located in the Mid-Atlantic United States. The power plant contains six 2 MW arrays, labeled here as array 1–array 6. The modules used in these arrays were 72-cell mono-Si modules of the same manufacturer and model, with a power rating of 325 W. The modules were assembled in at least three different facilities, and the only outwardly noticeable difference in bill of materials was the front glass. The modules are ground mounted south-facing at fixed tilt.

Outdoor IV characterization and field EL imaging was performed on a subset ($<$1%) of the modules in each array, and these measurements were used to select modules for laboratory analysis. A total sample size of 224 modules was used to help mitigate statistical uncertainty. IV curves were corrected to standard test conditions, with corrections made for irradiance, angle of incidence, temperature, soiling, and series resistance. A subset of the tested modules was also imaged by EL in the field. This field testing was carried out in an 18-hour period with all the modules mounted in place. Histograms

M.G. Deceglie, T.J Silverman, S. W. Johnston and I. L. Repins are with the National Renewable Energy Laboratory, Golden, CO, USA. J. Rand and M. Reed are with Core Energy Works, Newark, DE, USA. R. Flottemesch is with Constellation, Baltimore, MD, USA. email: michael.deceglie@nrel.gov

Manuscript received January 2020

of the irradiance- and temperature-corrected power measured from the field IV curves are shown in Fig. 1. A substantial range in individual module performance was indicated by the field testing. We observed that modules from array 1 were on average higher-performing compared to those in arrays 2-6. These differences in IV performance correlated with reduced brightness in the EL images. Performance was not correlated with position within a string; some strings were entirely high performing, some entirely low performing, and some mixed. Example EL and IV results from a single string with both low and high performance is shown in Fig. 2. Based on the IV and EL observations along with technology vintage, LeTID was suspected. The field testing facilitated identification of a small number of samples for detailed laboratory analysis at NREL to verify the degradation mechanism(s). Three categories of modules were selected for further analysis:

A) Typical modules from array 1. These were selected to have P_{mp} values close to the median P_{mp} for array 1. These were high-performing compared to other arrays.
B) Typical modules from arrays 2–6. These were selected to have P_{mp} values close to the median P_{mp} for arrays 2–6. These were low-performing compared to array 1.
C) Atypical high-performing modules from array 2–6. These had high-performance relative to modules typical of arrays 2–6

Two modules from each category above were selected for further analysis in the laboratory at NREL. Before selecting specific modules, the EL images were examined to ensure that the candidate module did not suffer from obvious cracked cells, or inactive cell strings. These six modules were delivered from the field along with two unfielded spare modules of the same type, for further laboratory study. For group B, we selected a module from array 2 and from array 3; time series analysis and the outdoor IV characterization revealed no substantial differences between arrays 2–6, enabling us to work with a lower number of modules rather than sampling from each array. At the time the modules were collected for laboratory study, the system had been in operation for approximately three years. Below, the modules are referred to by array number and replicate. For example, module 2.1 originates from array 2, and is the first module from that array. Unfielded control modules are assigned to array 0.

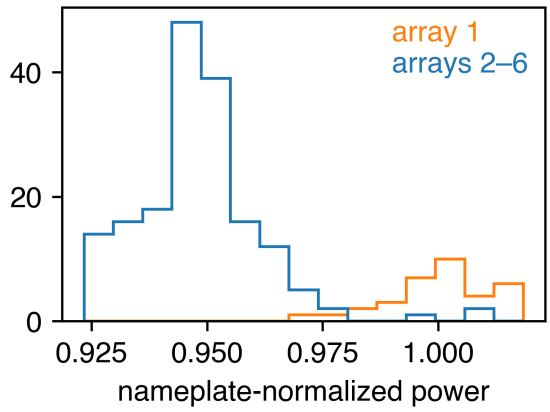

Fig. 1. Histograms of normalized power for modules from array 1 (orange) and arrays 2–6 (blue) based on corrected field IV curves. The modules in arrays 2–6 tend to be more degraded than those in array 1.

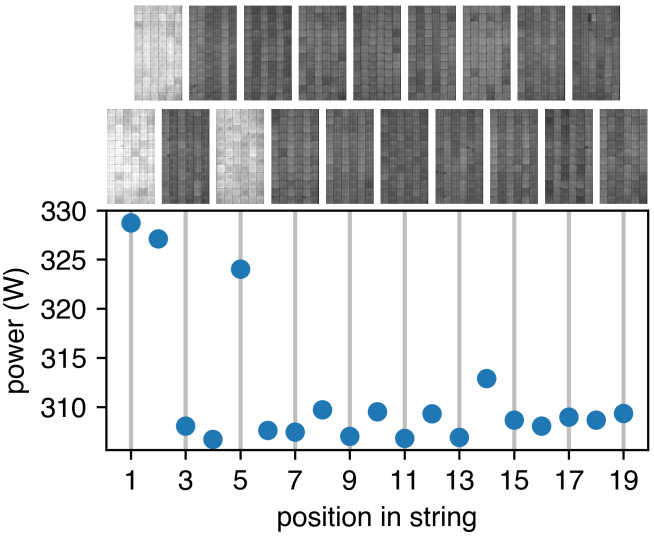

Fig. 2. Module power as a function of electrical position in a string from array 2 along with field EL images. EL images are centered on the x axis with respect to their electrical position. Modules in position 1, 2, and 5 show have both higher power and brighter EL images. Correlation between EL and IV measurements further supported the conclusion that degradation was affecting some modules in the array, but not others.

III. Methods

A. Operational time series analysis

We assessed the degradation in the energy generation of the system by analyzing time series operational data from the power plant. The time series consists of various meteorological and electrical measurements, recorded in averaged 15 minute intervals. In this study we used measurements of plane-of-array (POA) irradiance, module temperature, and energy output. POA irradiance was measured across the site by seven reference cells and two thermopile pyranometers. Module temperatures were measured by a probe on the back of modules, with one module temperature measurement per array, for a total of six. For both POA irradiance and module temperature, we took the median of all the measurements at each time step. This ensures that a common set of reference conditions are used for all the arrays, and that differences in sensors do not contribute toward differences in observed degradation rate. PV energy generation was obtained from energy meters, with one meter associated with each array.

Irradiance measurements can drift over time contributing to bias in calculated degradation rates [7]. To mitigate this effect, we corrected the median value of POA irradiance according to satellite irradiance data. Satellite reanalysis data for hourly direct normal irradiance (DNI), global horizontal irradiance (GHI), and diffuse horizontal irradiance (DHI) were obtained for the location of the plant [8] and transposed to plane of array using an isotropic sky model with an albedo of 0.25 [9]–[11]. This satellite POA irradiance was then aggregated daily and

compared to the daily aggregated insolation calculated from the median measured POA irradiance. The daily ratio of satellite POA to measured POA was regressed over the period of study via the Theil-Sen method [12] to obtain a linear correction factor that was then multiplied by the median measured POA. The slope of this correction was 0.73%/day. This corrected value of POA was used for calculation of degradation rates.

The degradation analysis was carried out with RdTools, an open-source python package for analysis of PV data [13]. The methods underlying RdTools have been described previously [7], [14], [15], but we review the methods briefly as they are implemented here. The first step is to normalize to a model; energy generation of PV for each time step is divided by the expected generation based on a simple irradiance and temperature coefficient model. The next step is to filter to eliminate erroneous (non-positive) energy generation values, POA irradiance outside the range of 200–1200 W/m^2, module temperature values outside the physically relevant range of -50–110°C, and inverter clipping. This was achieved with RdTools filters configured with their default values [13]. The next step is to aggregate the normalized and filtered performance to daily frequency using an insolation-weighted mean. We then filtered the daily values for outliers according to the upper and lower Tukey fences, that is, 1.5 times the interquartile range above and below the first and third quartiles respectively [16]. The final step is to perform the year-on-year calculation [17], which estimates the degradation rate as the median value of all slopes drawn between two daily points separated by exactly one year. We report the median (P50) and the 95% confidence interval for the median. Generally, at least two years of data is required for the year-on-year approach, with improved results for longer data sets.

B. Accelerated testing

To determine whether the degradation kinetics where consistent with LeTID, we performed accelerated testing at NREL. Module 2.1 was subjected to two sets of accelerated test conditions known to promote light and elevated temperature degradation (LeTID) and subsequent regeneration [18], [19]. The rates of degradation and recovery in response to different stress levels enabled us to test whether the observed degradation was consistent with LeTID. In the first phase, termed the "degradation phase," the module temperature is controlled to 75°C, while current is applied in the dark. The applied current, I_{app}, is equal to the difference between the module STC short-circuit current, I_{sc}, and maximum power current, I_{mp}, i.e. $I_{app} = I_{sc} - I_{mp}$. Use of this relatively small forward current slows degradation to the point where it can be measured by weekly module light IV curves and EL imaging. In the second phase, termed "regeneration phase," temperature is increased to 85°C, and applied current is increased to $I_{\mathrm{app}} = I_{\mathrm{sc}}$. Weekly module light IV curves and EL imaging are also performed during the degradation phase. Typically, each phase consists of four one-week intervals with intervening IV measurements and EL imaging. In this study, we carried out two one-week intervals in the degradation phase, followed by three one-week intervals in the regeneration phase. All steps were executed with a module temperature tolerance of ± 3°C, with one hour temperature ramps during which no bias was applied.

LeTID degradation and regeneration are both accelerated by injected current and elevated temperature. However, the degradation process is much faster than the regeneration process. Thus, while both the degradation and regeneration phases utilize heat and current, lower values are applied during the degradation phase so that the realized rates of degradation and regeneration facilitate weekly characterization.

C. Laboratory module and cell current voltage measurements

Laboratory IV curves were collected using a commercial class AAA pulsed solar simulator. We measured IV curves for each of the modules on receipt from the field, after cleaning them to remove soiling. For module 2.1, which underwent accelerated testing, IV curves were repeated after each step of the accelerated test. The module IV curves were collected at 25.0$\pm$0.5°C and 1000 W/m^2. We also collected cell-level IV curves on selected cells from module 2.1 (after accelerated testing) and 3.1 (as received). Cell-level curves were taken at at 25.0$\pm$0.5°C and multiple irradiances of 200, 400, 600, 800, and 1000 W/m^2. Electrical contact was made to individual cells by grinding away the backsheet and back encapsulant over each of the ribbons within the module and connecting them together by soldering bus ribbon to them. Probing the bus ribbon tabbed from bus bars exposed on either side of a cell of interest enabled us to obtain single cell IV curves. We fitted single-diode models to each cell's I-V curves using the SDM-G algorithm [20]–[22]. This method uses information from multiple I-V curves, in this case taken at multiple irradiance levels, to fit a single equivalent circuit model.

D. Laboratory photoluminescence imaging

We collected high resolution PL images of each module as received at NREL. PL imaging uses light to excite excess carriers in the solar cells and then PL is collected by a camera. For PL imaging, optically excited carriers are uniformly injected throughout the cell which diminishes effects of series resistance that may influence voltage and carrier distributions when collecting EL images using rated current values. We collected PL images cell-by-cell. In the system used here, the light source consisted of two laser diodes at a wavelength of 808 nm. The light was fiber coupled from the laser diode units and was spread out over an oversized area of one solar cell that is approximately 16×16 cm. The laser illumination was coupled out of the optical fibers using a collimator and engineered diffuser. We adjusted the laser power and optics to output 25 mW/cm2, roughly 1/4 Sun intensity, with a uniformity over the cell area of less than 5% variation. We collected PL images using a silicon-detector camera with a long-pass filter on the lens to block the 808-nm laser light but transmit the longer wavelength PL. Typical exposure times were 5 to 10 seconds per cell. Automated stages moved the module from cell to cell under the field of view of the camera, and PL images are collected on each cell giving a resolution of roughly 1000 x 1000 pixels per cell. The

resulting module PL image was composed of a series of cell images that total to the number of cells within the module. The PL images were corrected for vignetting, the lower intensity of the image corners due to camera and lens artifacts, by dividing each image by a normalized image collected using uniform emission from an integrating sphere. Finally, the cell images were cropped and stitched together to give a single high-resolution PL image of the module.

After closely cropping PL images to each include only a single cell, we evaluated each cell's median PL intensity. We then used *k*-means clustering to divide the 144 cells from both degraded modules (2.1 and 3.1) into two populations: low PL intensity and high PL intensity. A cell's PL intensity is correlated with its V_{oc}[23], so these two populations were intended to cover the high-performing and low-performing cells in the modules.

E. Laboratory electroluminescence imaging

While collecting PL cell-by-cell as described in Section III-D provides a high-resolution data set, it is time consuming. To expedite characterization between steps of accelerated testing, we used EL imaging of the entire module during laboratory testing at NREL. Before testing and between steps of accelerated testing, we collected EL images of the entire module under test. We forward-biased the module to pass approximately 10% of its nameplate I_{sc} and collected images using a cooled silicon CCD camera. We applied flat-field correction to the EL images and we aligned images using the edges of the individual cells.

IV. Results

A. Initial characterization and effects of field service

The normalized daily performance of each array used in the degradation analysis is shown for each array in Fig. 3 and the extracted degradation rates are shown in the top panel of Fig. 4. We observe that arrays 2–6 degrade significantly more rapidly than array 1 based on a set of two-sided Mann-Whitney tests between all the year-on-year slopes from array 1 and those from each other array, which yield p-values less than 1×10^{-5}. We note that array 1 shows a positive P50 rate of change (Fig. 4), but with a confidence interval that encompasses zero. Though the satellite correction of POA irradiance was found to mitigate the positive bias to some extent, a small bias remains. Possible explanations for this include drift in sensors or the median module temperature at the site becoming less representative of the module temperatures in array 1 as the other arrays degrade. For the purposes of this study, we are less concerned with the absolute value of the degradation rate than with the relative degradation rate between arrays. Since we use the same module temperature and POA irradiance to extract degradation for every array, we can confidently conclude that arrays 2–6 are producing less energy over time when compared to array 1.

IV curves collected on modules returned from the field from categories A and B (Table I) corroborate the observation from both field characterization and time series analysis that arrays 2–6 degraded more rapidly compared with array 1.

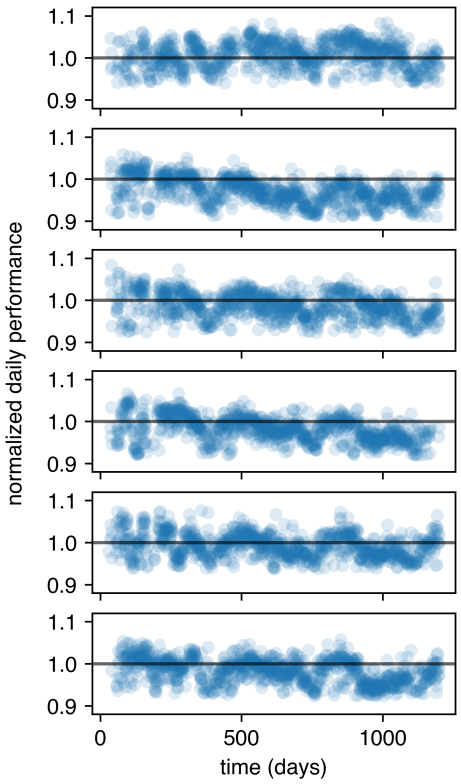

Fig. 3. Normalized daily performance of each sub array (1–6, top to bottom) in the system.

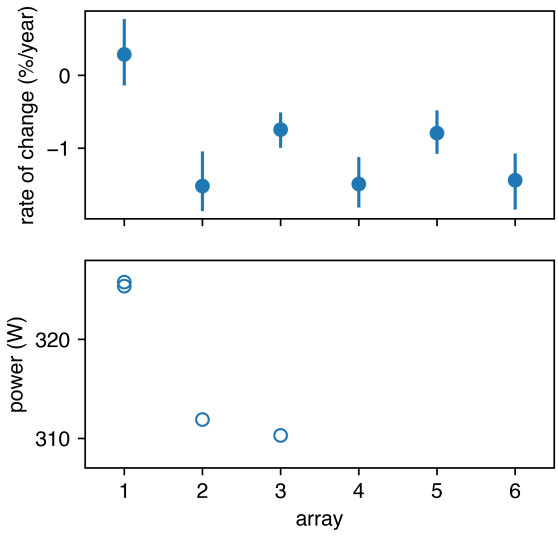

Fig. 4. Top: Results of year-on-year degradation analysis of each array. Points indicate the P50 rate of change, and lines indicate the extent of the 95% confidence interval. Negative rate of change denotes degradation. Bottom: Power of fielded modules from the system based on IV measurements taken at STC, plotted according to the array from which the modules were collected. Only category A and B modules are shown (modules 1.1, 1.2, 2.1, 3.1).

The absolute uncertainties for the values listed in Table I are ±2.5% for P_{mp}, ±0.6% for V_{oc}, and ±2.4% for I_{sc}. However, the precision for the purposes of comparing parameters between curves is estimated to be approximately 0.1% for I_{sc}, and 0.2% for P_{mp} and V_{oc}. The STC P_{mp} values for these modules are also plotted in Fig. 4. The results in Table I also agree with the field IV curves, indicating that modules in arrays 2–6 were not uniformly degraded, with some (atypical high performers, category C) performing similarly to the array 1 modules. We also observe that unfielded modules had P_{mp} values greater than nameplate.

Fig. 5 presents PL measurements made on fielded modules as received from the field. We observe that modules 2.1 and 3.1 are substantially darker than the array 1 modules and the array 2–6 atypical high-performing modules. We also observe that in all 4 high-performing modules substantial cell-to-cell variability is observed. These observations are consistent with observations from field EL. This indicates that cell-to-cell variability in luminescence is not easily interpretable as an indicator of susceptibility to the degradation mode observed here.

PL imaging on as-received modules also revealed a back contact pattern consistent with localized back contacts (e.g. PERC) on all modules except 2.1 and 3.1. The differences in back contact were confirmed by visual inspection of the back contacts of cells in modules 3.1 and 1.1 after removal of the back encapsulant from a small region. Back contact technology should not be taken as a general indicator of susceptibility because LeTID has been observed on a wide variety of cell types [2], [4]–[6]. However, in this study, it corresponds to an observed physical difference between two populations.

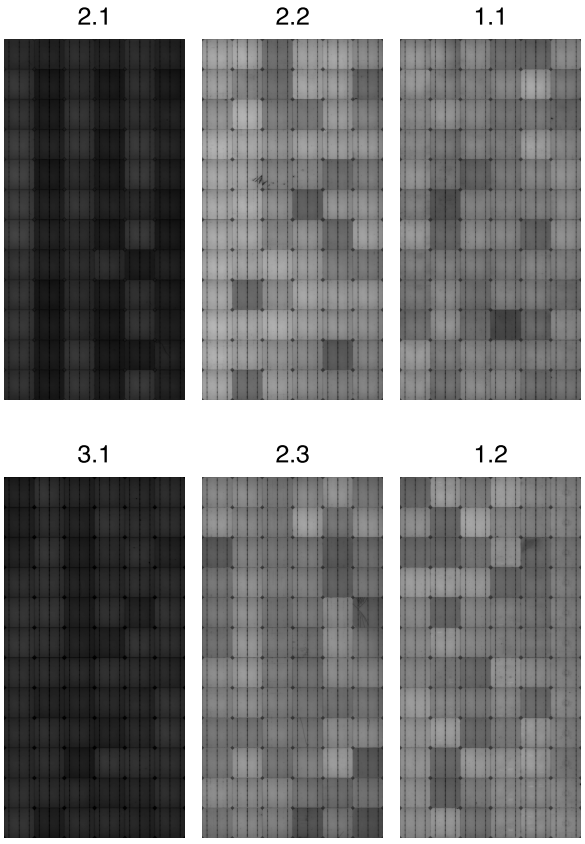

Fig. 5. Photoluminescence images of fielded modules. Module labels appear above each image. Modules 2.1 and 3.1 which were chosen to be typical of the affected arrays are darker than the unaffected modules. We note substantial cell-to-cell variation in brightness, even among the unaffected modules.

TABLE I
IV MEASUREMENT SUMMARY

module	P_{mp} (W)	V_{oc} (V)	I_{sc} (A)	FF(%)	category
1.1	326	46.3	9.4	75.0	A
1.2	325	46.4	9.4	74.5	A
2.1	312	45.4	9.1	75.4	B
3.1	310	45.6	9.0	75.3	B
2.2	328	46.5	9.4	75.0	C
2.3	327	46.2	9.4	74.9	C
0.1	333	47.0	9.5	74.6	
0.2	335	47.0	9.5	74.7	

Note: Categories are defined in Section II.

B. Effects of accelerated testing

The changes in STC IV parameters and EL with each week of accelerated testing are shown in Fig. 6 for module 2.1, which was a chosen as a typical degradation-affected module. Results from a Si control module of different make and model that underwent IV characterization alongside module 2.1, but that was not exposed to any accelerated testing, indicated precision in parameters extracted from the repeated IV curves of 0.1% for I_{sc}, and 0.2% for P_{mp} and V_{oc}. We observe small improvements in performance for the degradation phase, followed by more substantial increases in the regeneration phase, with the largest gain in the first step of the regeneration phase. Fig. 6 also shows that EL became more uniform and brighter as the module performance improved.

The same effect on luminescence is more precisely quantified with EL results in Fig. 7 on the same module. We observe that all cells became brighter and the distribution of EL intensities became tighter (the largest changes in brightness occurred in cells that were originally dim). The change in the median EL intensity across the entire module was +60%.

A comparison between single-cell IV curves from module 3.1 as received from the field and module 2.1 after all five steps of accelerated testing is shown in Fig. 8. The figure distinguishes between two populations of cells based on PL imaging on both modules as received: those that were bright and those that were dim. For module 3.1 as received, we note that the dim cells tended to exhibit lower V_{oc}, higher ideality factor, and higher saturation current density. All three trends are consistent with the dimmer cells being lower quality. Module 2.1, after regeneration, exhibits improvements (relative to module 3.1 as received) and much tighter groupings in the saturation current density and ideality factor. The V_{oc} of the individual cells is also higher for module 2.1 regenerated, but the grouping is not substantially tighter.

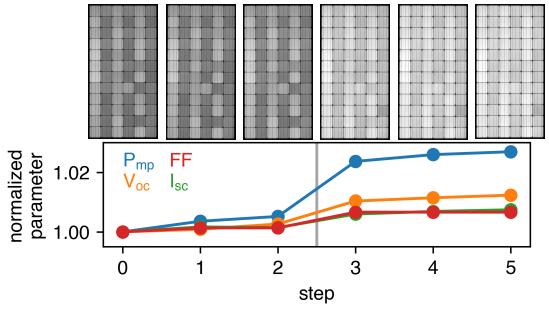

Fig. 6. The plot shows relative changes in the STC IV parameters of module 2.1 when exposed to accelerated testing. Electroluminescence images collected at approximately $0.1 \times I_{sc}$ are shown above the plot corresponding to the step indicated by the the x-axis. Steps 1 and 2 were the degradation phase, steps 3–5 were the regeneration phase. All measurements and images are plotted according to the accelerated testing step after which they were collected.

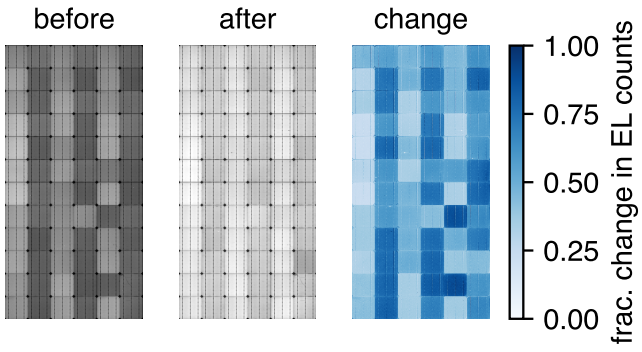

Fig. 7. Changes in electroluminescence at approximately $0.1 \times I_{sc}$ of module 2.1 with accelerated testing. "After" denotes after all five steps of accelerated degradation and regeneration testing.

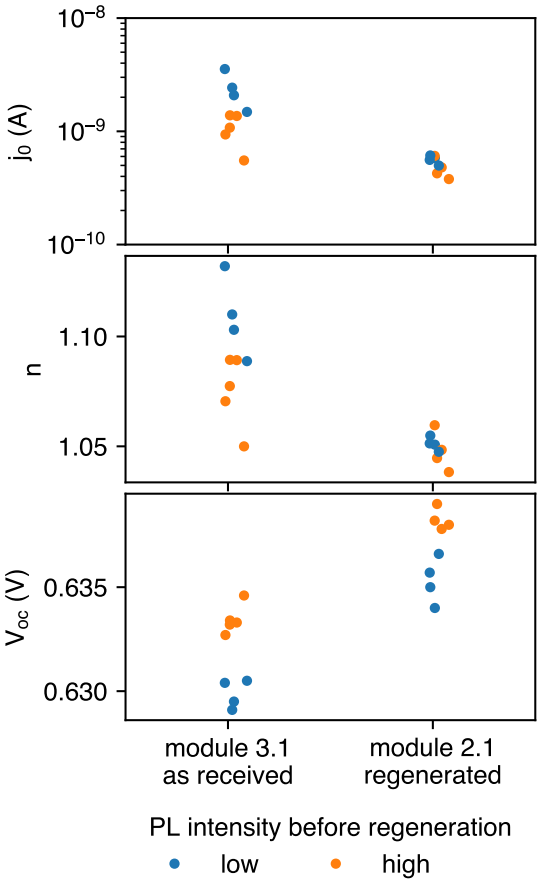

Fig. 8. Comparison of saturation current (top), diode ideality factor (middle), and V_{oc} (bottom) of single cells from module 3.1 as received from the field, and module 2.1 after accelerated testing. Points are colored according to a grouping by photoluminescence intensity from photoluminescence measurements taken on both modules in the as-received state. The module which underwent accelerated testing (2.1) shows a tighter distribution in saturation current and ideality factor, and improved values for all three parameters.

V. Discussion

The data show that arrays 2–6 within the system degraded more rapidly than array 1. IV curves on modules returned are consistent with this conclusion, but also indicate that modules within arrays 2–6 were not universally degraded. Anecdotally, we observed different back contacts on modules 2.1 and 3.1 (as described in Section IV-A), compared to the other modules in this study. This suggests that differences in cell processing (but not necessarily the contact technology itself) caused differences in susceptibility to the observed degradation. It was likely a logistical coincidence that the majority of unaffected modules were installed in array 1.

The data on the two affected modules returned from the field suggest that a substantial portion of the observed degradation in these fielded modules is due to LeTID. This conclusion results from a comparison of several characteristics of the fielded modules with those of other modules known to exhibit LeTID.

The expected characteristics of a module that exhibits LeTID are as follows:

1) **Time scale in accelerated test:** In accelerated tests with conditions described earlier in Section III-B, LeTID degradation and regeneration each occur over several weeks.
2) **Effect of current and temperature:** Both degradation and regeneration processes are accelerated by applying higher current and temperature.
3) **Variation from cell to cell:** EL images of modules with LeTID tend to show variation from cell to cell [3], [24], [25]. This variation is accentuated when the module is in the LeTID degraded state, and less apparent when the module is in the initial or regenerated states. The cell-to-cell variation may result from the position within the ingot from which the cell originates [26]–[28] variations in SiNx thickness, or variations in firing maximum temperature [29]–[33] or ramp rates [30], [34].
4) **Slow degradation in field:** LeTID degradation occurs on a time scale of years in the field. The only published study of fielded modules with LeTID to date shows modules maximum degradation in the field occurring at 3 years for a sunny climate, and slower for a cooler climate [35].

Fig. 3 allows an examination of the degradation rate. While outdoor data are influenced by many factors that convolute climactic conditions with apparent performance, the slow

nature of the degradation is apparent. For arrays two, four, and six, which have the highest degradation rates, Fig. 3 indicates that degradation is still occurring in the two- to three-year time frame. This time frame is roughly consistent with LeTID characteristic 4 in the list above. Additionally, this time frame allows us to rule out boron-oxygen light induced degradation (B-O LID) as a cause for the decreased system, since B-O LID causes degradation within days [36].

Regeneration during accelerated test also occurs on the time scale expected for LeTID (characteristic 1). Under regeneration accelerated test conditions (to the right of the dotted line in Fig. 6), module performance increases over the course of four weeks, with most of the increase occurring in the first week.

An obvious difference between the data of Fig. 6 and accelerated tests performed on published studies of pristine modules is that there is no degradation in the initial portion of the test (to the left of the dotted line in Fig. 6). No degradation occurs because the module in the accelerated test already degraded in the field (Fig. 3 and Fig. 4). Instead, a small amount of regeneration begins to occur in the fully degraded module at the beginning of the accelerated test. This initial regeneration occurs more slowly than that occurring after step two, since the test conditions are switched to higher current and temperature after step two. Thus, the increased rate of regeneration between steps 2 and 3 is consistent with the behavior of modules with LeTID (characteristic 2).

The progression of the module's EL image during accelerated testing, shown in the upper portion of Fig. 6, shows a progression from larger to smaller cell-to-cell differences as the sample regenerates. This progression is consistent with that observed in modules with LeTID (characteristic 3).

The lack of degradation in accelerated test (Fig. 6) implies that the deployed modules entered the fully degraded LeTID state during three years in the field. This implication may be reasonable. A published study shows modules degrading over three years in Cyprus [35]. However, the modules in this study were deployed in a less sunny climate. The temperature and irradiance conditions experienced by modules in this study are shown in Fig. 9. For modules installed at optimum fixed tilt, and using typical meteorological year climate data [37], it is calculated that the yearly plane of array incident energy in Cyprus is 2100 kWh/m^2, whereas it is 1600 kWh/m^2 for the deployed modules in this study. It is important to consider, however, that some events may accelerate the degradation. First, because LeTID is accelerated by excess carrier concentration, degradation occurs much faster ($\sim$10x) when there are periods of time that the module is illuminated and at open-circuit. Such times may include during system construction but prior to grid connection, daily when the irradiance is low enough that the inverter has not yet turned on, or if the inverter is off due to system maintenance or repair. Second, comparison of LeTID degradation rates between sites where different module types are installed must take into account differences in module characteristics and operating point (e.g. when inverter clipping occurs) both of which can result in different excess carrier concentrations and thus different LeTID degradation rates. Fill factors and operating points of the modules in the Cyprus study are not published.

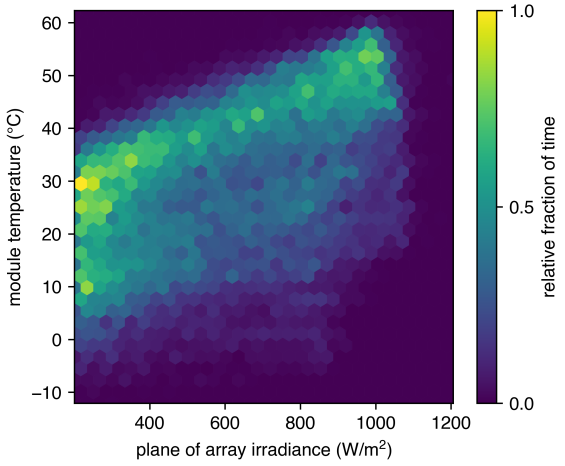

Fig. 9. Hexagonally-binned two dimensional histogram showing the relative fraction of time the modules in the system were experienced different irradiance and module temperatures, based on field-recorded data for points observed above 200 W/m^2 plane of array irradiance.

VI. Conclusion

We have described an instance of apparent LeTID in an utility scale system along with a process to identify and diagnose defective modules in the field. The observations and methodology documented here will help diagnose other instances of LeTID. However, it is important to note that LeTID is not yet fully understood and there may be variation in the degradation kinetics between different products.

Modules at the site from this study are not uniformly affected by the degradation. Whether the modules were affected or not corresponded with the type of back contact we observe on the cell. This highlights the level of difficulty presented when variations in the module BOM are present. In this case the variation had a significant impact to field performance even though the modules were from the same manufacturer, manufactured at roughly the same time, had the same model number, and had the same outward visible appearance. This underscores the importance of a robust quality program on the part of manufacturers and the importance of re-qualification of modules when changes are made to the cells, materials, or manufacturing processes associated with a module model. The results also give critical feedback to module manufacturers and improve system owners' ability to predict performance.

The holistic methodology used here combines results from field characterization, time series analysis, and detailed study of samples returned from the field. Field testing of a small fraction ($<$1%) of modules enabled us to identify samples to bring back to the laboratory. We then used accelerated stress, luminescence imaging, and IV measurements on these modules to identify the degradation mechanism without testing an excessive number of modules in the laboratory. Applying this approach to contemporary systems that exhibit under performance is an important part of of ongoing reliability efforts in the PV community. Learnings from such studies

inform the standards making process by identifying gaps in standards or problems with their application.

Acknowledgment

The authors would like to thank Kent Terwilliger, Helio Moutinho, Steve Rummel, Allan Anderberg, and Joshua Morse for help with laboratory characterization and Teresa Barnes for guidance and feedback on the study. The authors would also like to thank the community for help in developing RdTools.

This work was authored in part by Alliance for Sustainable Energy, LLC, the manager and operator of the National Renewable Energy Laboratory for the U.S. Department of Energy (DOE) under Contract No. DE-AC36-08GO28308. Funding provided by the U.S. Department of Energy's Office of Energy Efficiency and Renewable Energy (EERE) under Solar Energy Technologies Office (SETO) Agreement Number 34357. The views expressed in the article do not necessarily represent the views of the DOE or the U.S. Government. The U.S. Government retains and the publisher, by accepting the article for publication, acknowledges that the U.S. Government retains a nonexclusive, paid-up, irrevocable, worldwide license to publish or reproduce the published form of this work, or allow others to do so, for U.S. Government purposes.

References

[1] *IEC 61215: Terrestrial photovoltaic (PV) modules - design qualification and type approval*, International Electrotechnical Commission, 2016.

[2] K. Ramspeck, S Zimmermann, H Nagel, *et al.*, "Light induced degradation of rear passivated mc-si solar cells," in *Proc. 27th Eur. Photovolt. Sol. Energy Conf. Exhib.*, vol. 1, 2012, pp. 861–865.

[3] F. Kersten, P. Engelhart, H.-C. Ploigt, *et al.*, "Degradation of multicrystalline silicon solar cells and modules after illumination at elevated temperature," *Solar Energy Materials and Solar Cells*, vol. 142, pp. 83–86, 2015.

[4] F. Fertig, K. Krauß, and S. Rein, "Light-induced degradation of pecvd aluminium oxide passivated silicon solar cells," *physica status solidi (RRL)–Rapid Research Letters*, vol. 9, no. 1, pp. 41–46, 2015.

[5] F Fertig, R Lantzsch, A Mohr, *et al.*, "Mass production of p-type cz silicon solar cells approaching average stable conversion efficiencies of 22%," *Energy Procedia*, vol. 124, pp. 338–345, 2017.

[6] T. Niewelt, F. Schindler, W. Kwapil, *et al.*, "Understanding the light-induced degradation at elevated temperatures: Similarities between multicrystalline and floatzone p-type silicon," *Progress in Photovoltaics: Research and Applications*, vol. 26, no. 8, pp. 533–542, 2018.

[7] D. C. Jordan, C. Deline, S. R. Kurtz, *et al.*, "Robust PV degradation methodology and application," *IEEE Journal of Photovoltaics*, 2018, ISSN: 2156-3381. DOI: 10.1109/JPHOTOV.2017.2779779.

[8] The Weather Company. Cleaned observation API documentation, [Online]. Available: http : / / cleanedobservations . wsi . com / documents / WSI % 20Cleaned % 20Observations % 20API % 20Documentation.pdf (visited on 08/23/2019).

[9] H. Hottel and B. Woertz, "Performance of flat-plate solar-heat collectors," *Trans. ASME (Am. Soc. Mech. Eng.); (United States)*, vol. 64, Jan. 1942.

[10] W. F. Holmgren, C. W. Hansen, and M. Mikofski, "Pvlib python: A python package for modeling solar energy systems.," *J. Open Source Software*, vol. 3, no. 29, p. 884, 2018.

[11] pvlib-python v0.6.3, [Online]. Available: https://github.com/pvlib/pvlib-python.

[12] P. K. Sen, "Estimates of the regression coefficient based on kendall's tau," *Journal of the American statistical association*, vol. 63, no. 324, pp. 1379–1389, 1968.

[13] RdTools. DOI: 10.5281/zenodo.1210316. Direct link to version used in this paper: https : / / github . com / NREL / rdtools / tree / d8909aebc07b8abb074ff363281ca148dcdb855e, [Online]. Available: https://github.com/NREL/rdtools.

[14] D. C. Jordan, M. G. Deceglie, and S. R. Kurtz, "PV degradation methodology comparison: A basis for a standard," in *2016 IEEE PVSC*, 2016, pp. 0273–0278. DOI: 10.1109/PVSC.2016.7749593.

[15] M. G. Deceglie, D. C. Jordan, A. Nag, *et al.*, "Fleet-scale energy-yield degradation analysis applied to hundreds of residential and nonresidential photovoltaic systems," *IEEE Journal of Photovoltaics*, vol. 9, no. 2, pp. 476–482, 2019.

[16] J. W. Tukey, *Exploratory Data Analysis*. Reading, Mass., 1977, vol. 2.

[17] E. Hasselbrink, M. Anderson, Z. Defreitas, *et al.*, "Validation of the PVLife model using 3 million module-years of live site data," in *2013 IEEE PVSC*, 2013, pp. 0007–0012. DOI: 10.1109/PVSC.2013.6744087.

[18] F. Kersten, P. Engelhart, H. Ploigt, *et al.*, "A new mc-si degradation effect called letid," in *2015 IEEE 42nd Photovoltaic Specialist Conference (PVSC)*, 2015, pp. 1–5. DOI: 10.1109/PVSC.2015.7355684.

[19] E. Fokuhl, T. Naeem, A. Schmid, *et al.*, "LeTID – a comparison of test methods on module level," in *European PV Solar Energy Conference and Exhibition*, vol. 36, 2019.

[20] M. Campanelli. PVfit, [Online]. Available: https://pvfit.com/.

[21] M. B. Campanelli and C. R. Osterwald, "Effective irradiance ratios to improve i–v curve measurements and diode modeling over a range of temperature and spectral and total irradiance," *IEEE Journal of Photovoltaics*, vol. 6, no. 1, pp. 48–55, 2015.

[22] M. B. Campanelli and B. H. Hamadani, "Calibration of a single-diode performance model without a short-circuit temperature coefficient," *Energy Science & Engineering*, vol. 6, no. 4, pp. 222–238, 2018.

[23] G Smestad and H Ries, "Luminescence and current-voltage characteristics of solar cells and optoelectronic

devices," *Solar energy materials and solar cells*, vol. 25, no. 1-2, pp. 51–71, 1992.

[24] M. Pander. Fraunhofer CSP presents LeTID-benchmark of PERC-modules, [Online]. Available: https://www.csp.fraunhofer.de/en/news/LeTID-Benchmark.html (visited on 09/18/2019).

[25] PI Berlin. Letid for investors, [Online]. Available: https://16iwyl195vvfgoqu3136p2ly-wpengine.netdna-ssl.com/wp-content/uploads/2019/02/Paul-Grunow-presentation.pdf (visited on 09/18/2019).

[26] R. Søndenå, H. Haug, C. C. You, *et al.*, "Evolution of defect densities with height in a hpmc-si ingot," in *AIP Conference Proceedings*, AIP Publishing, vol. 2147, 2019, p. 140 010.

[27] M. Wagner, F. Wolny, M. Hentsche, *et al.*, "Correlation of the letid amplitude to the aluminium bulk concentration and oxygen precipitation in perc solar cells," *Solar Energy Materials and Solar Cells*, vol. 187, pp. 176–188, 2018.

[28] D. Chung, C. Chan, B. Mitchell, *et al.*, "Effect of wafer position in ingot on the light and elevated temperature induced degradation (letid) of multicrystalline silicon," in *2018 IEEE 7th World Conference on Photovoltaic Energy Conversion (WCPEC)(A Joint Conference of 45th IEEE PVSC, 28th PVSEC & 34th EU PVSEC)*, IEEE, 2018, pp. 0303–0308.

[29] M. Kim, S. Wenham, V. Unsur, *et al.*, "Impact of rapid firing thermal processes on meta-stable defects: Preformation of the letid and the suppression of bo defects," in *2018 IEEE 7th World Conference on Photovoltaic Energy Conversion (WCPEC)(A Joint Conference of 45th IEEE PVSC, 28th PVSEC & 34th EU PVSEC)*, IEEE, 2018, pp. 0341–0346.

[30] C. E. Chan, D. N. Payne, B. J. Hallam, *et al.*, "Rapid stabilization of high-performance multicrystalline p-type silicon perc cells," *IEEE Journal of Photovoltaics*, vol. 6, no. 6, pp. 1473–1479, 2016.

[31] D. Chen, M. Kim, B. V. Stefani, *et al.*, "Evidence of an identical firing-activated carrier-induced defect in monocrystalline and multicrystalline silicon," *Solar Energy Materials and Solar Cells*, vol. 172, pp. 293–300, 2017.

[32] D. Bredemeier, D. C. Walter, and J. Schmidt, "Lifetime degradation in multicrystalline silicon under illumination at elevated temperature: Indications for the involvement of hydrogen," in *AIP Conference Proceedings*, AIP Publishing, vol. 1999, 2018, p. 130 001.

[33] S. Zhang, J. Peng, H. Qian, *et al.*, "The impact of thermal treatment on light-induced degradation of multicrystalline silicon perc solar cell," *Energies*, vol. 12, no. 3, p. 416, 2019.

[34] H. C. Sio, H. Wang, Q. Wang, *et al.*, "Light and elevated temperature induced degradation in p-type and n-type cast-grown multicrystalline and mono-like silicon," *Solar Energy Materials and Solar Cells*, vol. 182, pp. 98–104, 2018.

[35] F. Kersten, F. Fertig, K. Petter, *et al.*, "System performance loss due to LeTID," *Energy Procedia*, vol. 124, pp. 540–546, 2017.

[36] K. Lee, M Kim, J. Lim, *et al.*, "Natural recovery from lid: Regeneration under field conditions," in *Proceedings of the 31st European Photovoltaic Solar Energy Conference and Exhibition-EU PVSEC, Hamburg, Germany*, 2015, pp. 14–18.

[37] JRC photovoltaic geographical information system, [Online]. Available: https://re.jrc.ec.europa.eu/pvg_tools/en/tools.html#TMY (visited on 09/18/2019).